Ocean Engineering 246 (2022) 110643

Contents lists available at ScienceDirect

Ocean Engineering

journal homepage: www.elsevier.com/locate/oceaneng

Development of a 3-legged jacket substructure for installation in the southwest offshore wind farm in South Korea

Thanh-Tuan Tran [a,b], Eungsoo Kim [c], Daeyong Lee [a,*]

[a] Institute of Offshore Wind Energy, Kunsan National University, Jeollabuk-do, Republic of Korea
[b] Advanced Structural Engineering Laboratory, Faculty of Civil Engineering, Ho Chi Minh City Open University, Ho Chi Minh City, Viet Nam
[c] Steel Solution Research Center, POSCO, Incheon, Republic of Korea

ARTICLE INFO

Keywords:
Jacket substructure
Pratt brace
Feasibility and sensitivity analyses
Design load cases
Environmental loads
Polar diagram

ABSTRACT

A suitable substructure for Offshore Wind Turbines plays an important role since it can efficiently reduce the financial costs of wind power projects. According to the track record of the Korean offshore wind farms, the 4-Legged Jacket (4LJ) substructure is the most utilized system; however, this design is still limited, specifically in the economic aspects. Thus, this study aims to design a more cost-effective substructure to enable large-scale deployment for Korean offshore projects. To achieve this objective, the new 3-Legged Jacket (3LJ) substructures together with various bracing topological forms (i.e., Pratt, Warren, and X-bracing) are developed. Results show that under the environment loads, dynamic responses obtained from the developed 3LJs are almost independent to the loading directionality; while there is a strong polarization in the case of 4LJ. Among the three cases of the 3LJs, the X-type topological form has the highest flexural stiffness together with the largest manufacturing and fabrication costs, while the Warren bracing system reaches ultimate strength earlier than the Pratt system. Therefore, the 3LJ substructure with a Pratt bracing system is suggested as a good alternative to the existing 4LJ system for Korean offshore wind farms, with reductions of up to 21% and 25% in total weight and number of weld joints, respectively.

1. Introduction

Designing substructure for Offshore Wind Turbines (OWTs) is a complex process due to simultaneous interactions of the environmental loads (i.e., aerodynamic, hydrodynamic). A suitable system plays an important role as it can efficiently reduce the financial cost of the wind power project. Until now, various types of substructures (i.e., monopile, jacket, tripod) have been developed mostly depending upon the water depth, and are widely installed in the world's offshore wind farms (Álamo et al., 2018; Bhattacharya S., 2019; Ju and Huang, 2019; Plodpradit et al., 2019; Tran et al., 2020a; Wu et al., 2019). However, according to the track records (Shi et al., 2015; Tran et al., 2020b), the jacket substructure is the most utilized system in South Korea due to its good performance in soft soils.

The jacket substructure is transferring the dynamic loads from the tower to the foundation. The typical concept is 4-Legged Jacket (4LJ) mounted on the piles or suction caissons. Among them, the jacket on piles, which is popularly adopted for the offshore wind turbines in South Korea, is known as the most considerable design due to the availability of installation vessels and driven equipment. However, this 4LJ design is still limited, specifically in the economic aspects in comparison with other substructures (Shi et al., 2013a, 2013b). Therefore, the development of a more cost-effective substructure to support existing OWTs is necessary.

In recent years, the 3-Legged Jacket (3LJ) substructure is evaluated as a more cost-effective system (Chew et al., 2014; Häfele et al., 2019). A comparative study between 4LJ and 3LJ was performed by Chew et al. (2014), and the outcomes indicated that the 3LJ is a more effective system for offshore wind. A similar study under FINO3 environmental conditions was also conducted by Häfele et al. (2019), and it showed that 3LJ is preferable to 4LJ. However, these researches have certain limitations on considering the effects of the bracing layouts on the dynamic performance of the jacket.

To consider the effects of bracing layouts on the dynamic performances of jacket substructures, a parametric study has been conducted by Puyang Zhang et al. (2020). They found that the X-brace jacket is better than other configurations, together with more material and construction costs. Similarly, Shi et al. (2015, 2013a) studied the dynamic characteristics of jacket substructures with various bracing systems.

* Corresponding author.
E-mail addresses: tranthanhtuan@kunsan.ac.kr, tuan.tth@ou.edu.vn (T.-T. Tran), eungsoo.kim@posco.com (E. Kim), daeyong.lee@kunsan.ac.kr (D. Lee).

https://doi.org/10.1016/j.oceaneng.2022.110643
Received 10 August 2021; Received in revised form 25 December 2021; Accepted 16 January 2022
Available online 4 February 2022

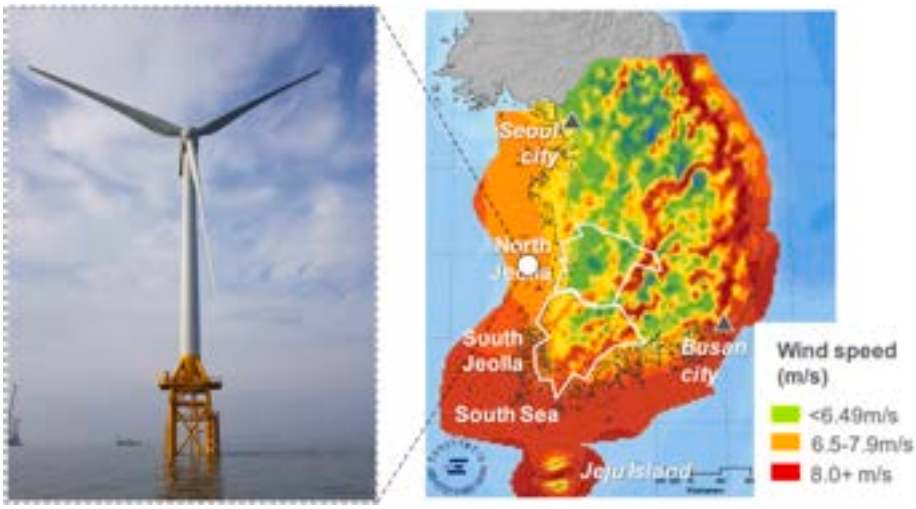

Fig. 1. 3 MW OWT used for this study (POSCO, 2017).

Table 1
Properties of the 3 MW reference wind turbine.

	Description	Unit	Value
Rotor-Nacelle-Assembly (RNA)	Rating		3 MW
	Rotor orientation	–	Upwind, 3 blades
	Mass of rotor	ton	64.6
	Mass of nacelle	ton	128.0
	Mass of RNA	ton	192.6
Tower	Bottom diameter	cm	450
	Bottom thickness	cm	3.4
	Top diameter	cm	307
	Top thickness	cm	1.8

Table 2
Environmental conditions (POSCO, 2017; Tran et al., 2021).

Description		Value	Unit
Wind	Wind speed in 50-year condition	42.50	m/s
Current	Velocity in 50-year condition (ECM)	1.04	m/s
	Velocity in NCM	0.96	m/s
Wave	Average water depth	14.00	m
	Significant wave height in 50-year condition	5.97	m
	Period in 50-year condition (T_{min}, T_{max})	8.66, 11.16	s

*ECM: Extreme Current Model; NCM: Normal Current Model.

They found that the smaller dynamic forces of Z-types can reduce structural fatigue as compared to X-type. However, these studies have not covered the impacts of critical loads such as Design Load Cases (DLCs) at the tower-substructure interface and extreme environmental loads (Env) acting on the substructures.

This work aims to develop a more efficient jacket substructure to support an existing 3 MW OWTs under the Korean environmental conditions, at a water depth of 14m. Through a proposed framework, preliminary geometries of the 3LJ substructures with different bracing topological forms (i.e., Pratt, Warren, and X-bracing) are firstly made based on the existing 4LJ-P (4-legged jacket with a Pratt bracing system) substructure. Feasibility and Sensitivity Analyses (FSA) are then performed for these concepts to find a more efficient configuration for reference 3 MW OWT. Finally, analysis outcomes (i.e., target frequency, dynamic responses under DLCs and Env) are discussed, and the reasonable jacket substructure is selected for the offshore wind farm in South Korea.

2. Wind turbine and design loads

2.1. Reference wind turbine

A typical 3 MW wind turbine installed in the Korean Southwest Sea, as illustrated in Fig. 1, is adopted in this research (POSCO, 2017). General specifications of the existing wind turbine are given in Table 1. The Rotor-Nacelle-Assembly (RNA) is located at the tower top with the corresponding mass of 192.6 ton. The total height of the tower is 56.77 m, and it is made of steel hollow tubes. The external diameters of the tower vary from 4.5 m (bottom) to 3.07 m (top), and their corresponding thicknesses decrease from 34 mm (bottom) to 18 mm (top), respectively.

2.2. Environmental loads (Env)

2.2.1. Environmental data

The environmental loads acting on the offshore structure can be classified into two groups: aerodynamic loads and hydrodynamic loads. Details of the environmental conditions are given in Table 2 (POSCO, 2017). In this study, the wind turbine class IIa corresponding to the 10-min reference wind speed of 42.5 m/s at the hub height is selected for designing OWT. In the case of hydrodynamic effects, the extreme condition in a 50-year return period is considered for both wave and current. The wave corresponds to the extreme wave load scenario, having a significant wave height $H_{s,50}$ of 5.97 m. The corresponding maximum wave height is a function of $H_{s,50}$, and is calculated using the relation of $H_{max} = 1.86H_{s,50}$. The current uses the constant profile along the water depth, with an average velocity of 1.04 m/s. Moreover, marine growth is also considered, with corresponding thicknesses of 5 cm–10 cm along the depth.

2.2.2. Definition of environmental loading directionality

Moreover, under the environmental condition, the structural response is sensitive to the loading directionality (Tran et al., 2020). Fig. 2a shows graphics of a jacket substructure subject to environmental loading conditions. The wave/wind/current loadings are applied simultaneously, and their angles with the structural system (x-axis) are denoted as α_{wind}, α_{wave} and $\alpha_{current}$, respectively. Different loading directionality ranging from 0° to 360° with a step of 15° are applied to the substructure, as indicated in Fig. 2b.

To evaluate dynamic responses of the structure under the environmental loading conditions, total displacement at the interface point (δ_{XY}) and maximum stress of the critical jacket leg members (σ) are selected. These engineering parameters are defined as the following equations:

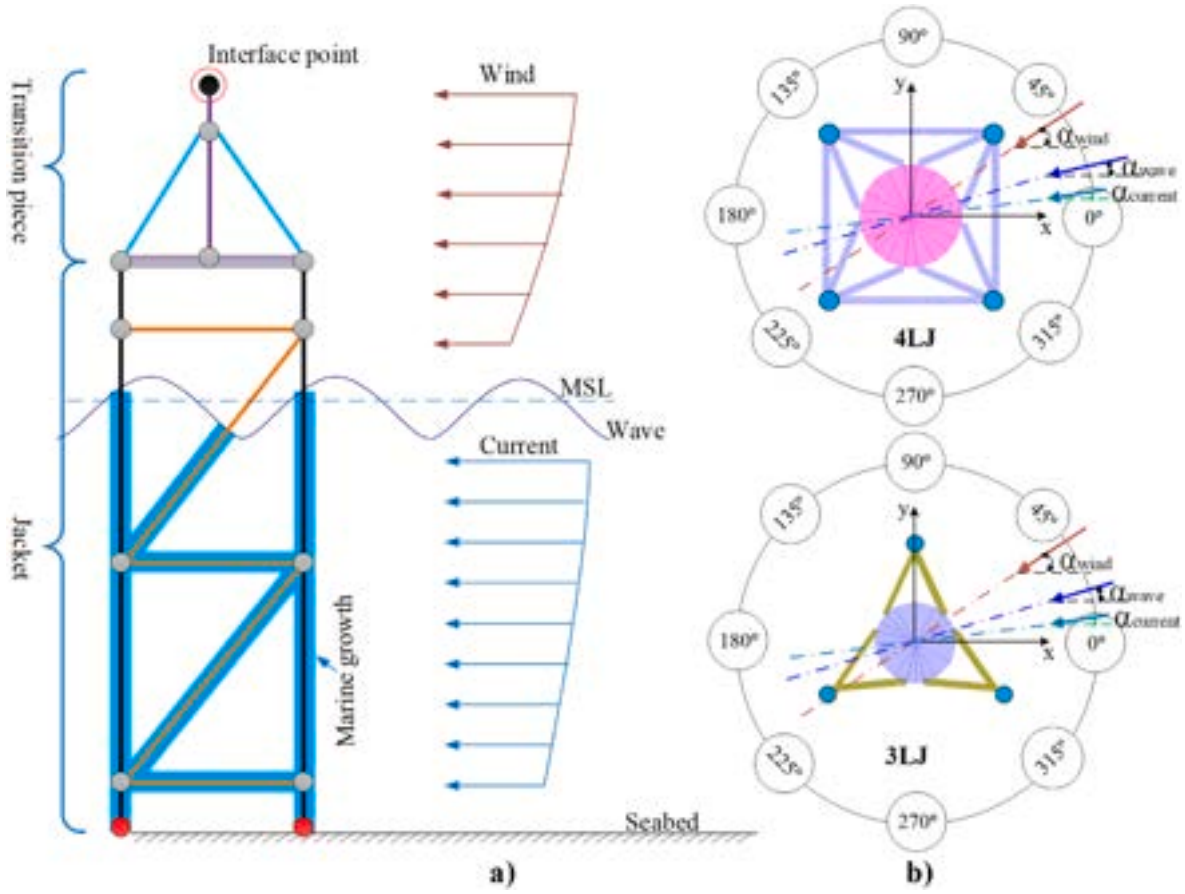

Fig. 2. (a) Environmental loads and (b) loading directionality.

Table 3
Design load cases at the interface point calculated from GH-Bladed.

DLC	Descriptions		Moment [kNm]		Force [kN]			
			Mx	***Fx***	***Fx***	***Fx***	***My***	***Mz***
DLC1	*Mx*	Max	49041.0	-2496.0	2173.3	-39.3	-958.5	-5207.5
DLC2		Min	-47885.0	-4998.1	-1731.4	-113.7	923.4	-5197.0
DLC3	*My*	Max	2369.3	45635.0	373.1	780.5	4.1	-6423.8
DLC4		Min	1038.0	-39301.0	-298.2	-699.3	49.3	-5167.9
DLC5	*Mz*	Max	6719.6	5033.7	5385.2	30.9	-145.7	-5243.5
DLC6		Min	-10207.0	-9978.7	-6124.0	-181.0	197.7	-5062.5
DLC7	*Fx*	Max	-23378.0	8965.3	-1222.2	1050.9	806.6	-4704.6
DLC8		Min	-22496.0	10333.0	-741.7	-978.1	-652.6	-4737.1
DLC9	*Fy*	Max	-19975.0	-10358.0	-1071.9	-713.9	1384.0	-4721.7
DLC10		Min	11407.0	1985.9	964.2	391.5	-1351.8	-4738.5
DLC11	*Fz*	Max	4275.3	3995.4	885.4	219.7	745.2	-4600.1
DLC12		Min	2281.6	37895.0	865.6	639.3	22.5	-7203.6

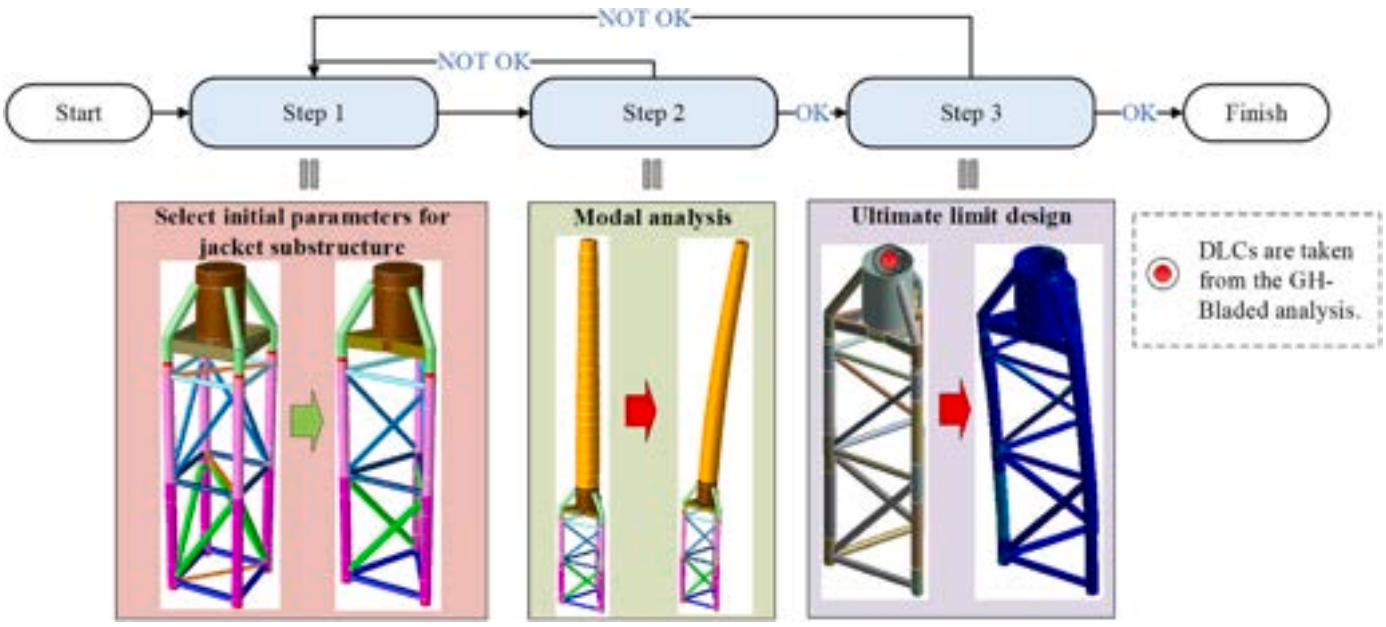

Fig. 3. Procedure of the 3-legged jacket development.

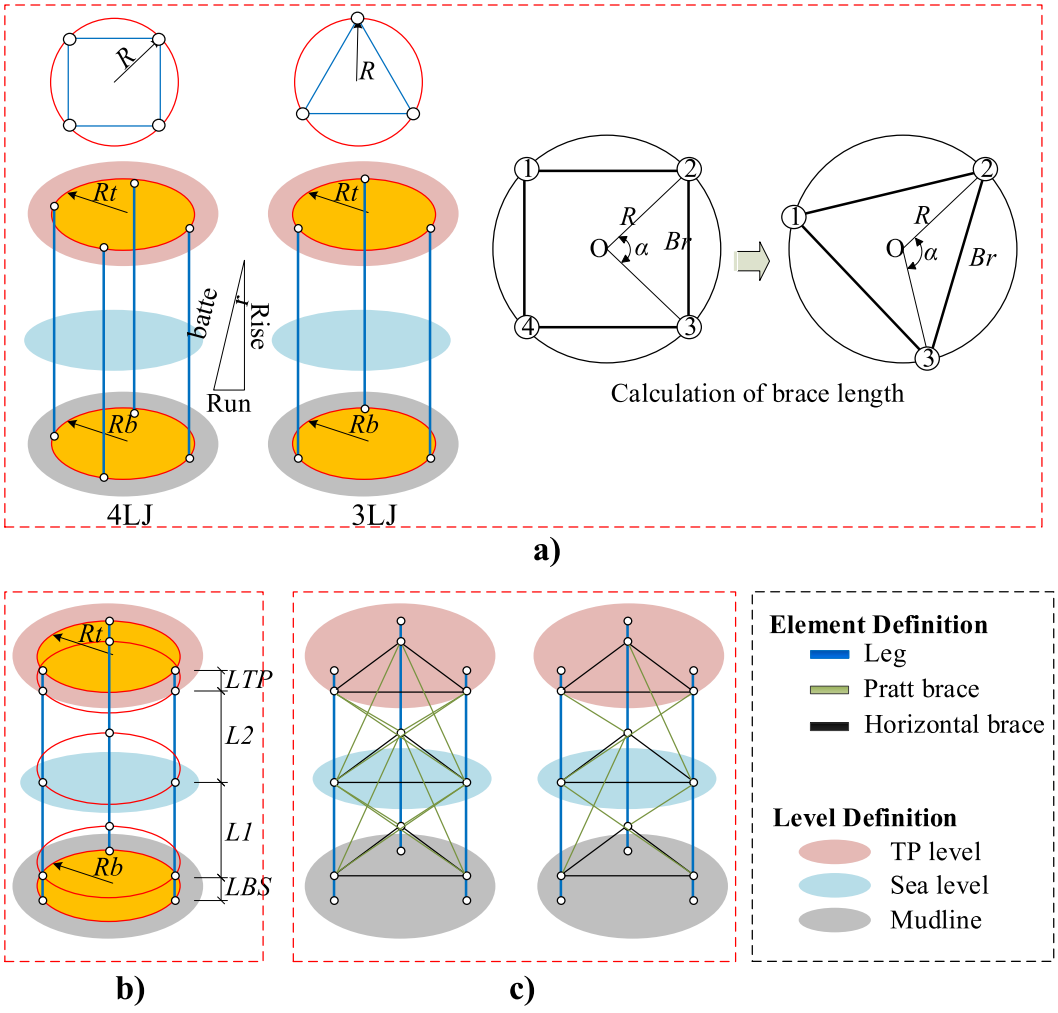

Fig. 4. 3-legged jacket design.

Table 4
Jacket properties [mm].

Component		4LJ-P		3LJ-P	
		Diameter	Thickness	Diameter	Thickness
Leg	LG	1047	16	1047	16
Horizontal brace	HB1	711	25	711	25
	HB2	609	19	609	19
	HB3	508	19	508	19
Vertical brace	VB1	711	22	711	22
	VB2	508	22	508	22
Joint can	JC1	1103	44	1103	44
	JC2	1079	32	1079	32
	JC3	1075	30	1075	30

$$\delta_{XY}(i) = \sqrt{\delta_X(i)^2 + \delta_Y(i)^2} \tag{1}$$

$$\sigma(i) = |\sigma_a(i)| + \sqrt{\sigma_{bx}^2(i) + \sigma_{by}^2(i)} \tag{2}$$

where $\delta_X(i)$ and $\delta_Y(i)$ are the response in X- and Y-direction at the angle i; σ_a is the axial, σ_{bx} and σ_{by} are bending major and bending minor stresses of the jacket members, respectively.

2.3. Design load cases (DLCs)

Twelve different design load cases defined by IEC 61400-1 (2005)

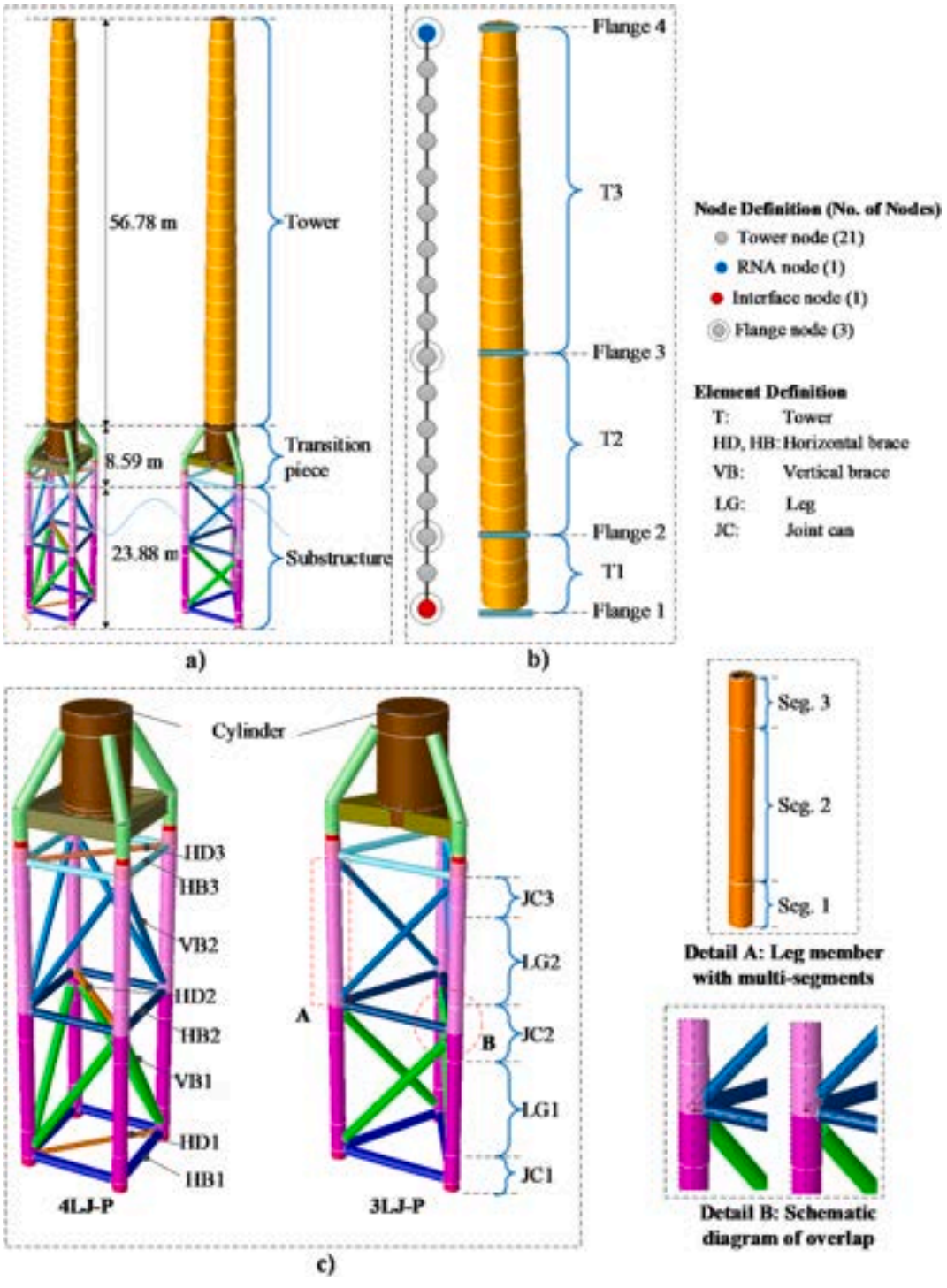

Fig. 5. Support structure modeling by SACS: (a) 3D, (b) tower, and (c) Jacket.

are utilized for the ultimate limit state (ULS) requirements. These DLCs are the combination of different wind and wave conditions and are taken from integrated time-domain simulations from the GH-Bladed (Bossanyi, 2010). The resulting forces and moments at the connection (interface point in Fig. 2a) between the tower and the transition piece are obtained and tabulated in Table 3. In this study, developed jacket substructures are checked with all DLCs for the ultimate design satisfaction.

3. Development of 3-legged jacket substructures

The jacket substructures considered in this work are designed to support a 3 MW reference wind turbine in South Korea at an average sea level of 14m. A framework for designing a new jacket substructure is graphically shown in Fig. 3. The detailed methodology proceeds in the below:

- Step 1: selecting an initial configuration of 3LJ through the proposed framework (Section 3.1). Based on the existing 4-legged jacket substructure (POSCO, 2017; Tran et al., 2021), 3-legged jacket configurations are newly developed.
- Step 2: conducting modal analyses for the full-3D OWT. This aims to check the target frequency of the developed support structures.
- Step 3: performing stress analysis under environmental and ultimate loading conditions. This aims to check the capacity of the selected members of the system.

  Step 2 and step 3 may require several iterations to obtain the optimized jacket substructure.

3.1. Preliminary geometry of jacket substructures

This section presents the process for developing a new 3-legged jacket configuration based on the existing 4-legged jacket. The schematic diagram of the 3-legged jacket design is illustrated in Fig. 4. Step-by-step of the methodology is described in the next subsections.

3.1.1. Shape of 3-legged jacket

Based on the existing 4LJ-P configuration, main parameters, such as the top radius (R_t), the bottom radius (R_b), and the total height of the jacket from the seabed to the transition piece (H_L), are extracted. The slope of the jacket leg (*batter*) is then defined as:

$$batter = \frac{Rise}{Run} = \frac{H_L}{R_b - R_t} \tag{3}$$

Notably, in Eq. (3), if the *Run* equals zero, the slope of the jacket (*batter*) is equal to zero.

According to the structural geometry of the existing 4LJ-P, the base and top radii are the same ($R = R_t = R_b$), leading to zero for the *batter*.

Consequently, the preliminary geometry of the 3LJ is developed under the same designing condition of *batter* $= 0$, as shown in Fig. 4a. The brace length (Br) is then calculated using the cosine law (Häfele et al., 2018):

$$Br = R\sqrt{2(1-\cos(\alpha))} \tag{4}$$

in which $\alpha = 2\pi/N_L$ (Fig. 4a) and N_L is number of the jacket legs.

3.1.2. Generation of jacket layers

Fig. 4b illustrates the procedure for generating the layers of the jacket. The lowest layer (L_{BS}) and air gap (L_{TP}) are determined first. The former is the distance between the seabed and the bottom horizontal brace. And the latter is the distance between the transition piece and the top horizontal brace, which is taken as $\geq 0.2H_{s,50}$ (significant wave height at 50-year return period) (Jalbi and Bhattacharya, 2020). The number of layers is defined to satisfy the requirements in NORSOK N-004 (2004). In particular, the angles between jacket leg and brace members should be ranged from 30 ° to 90 °.

3.1.3. Bracing system for the jacket

After obtaining the layers of the jacket substructure, three different bracing systems (i.e., Pratt, Warren, K-brace, or X-brace) are adopted to configure the jacket layouts. The obtained configurations are shown in

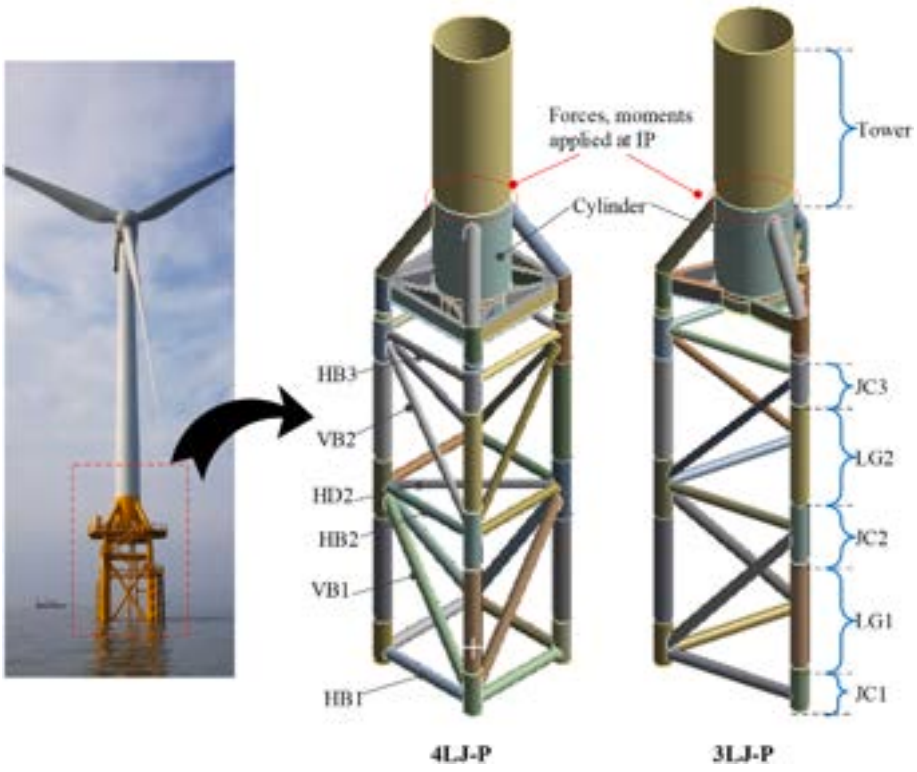

Fig. 6. Jacket modeling by ANSYS.

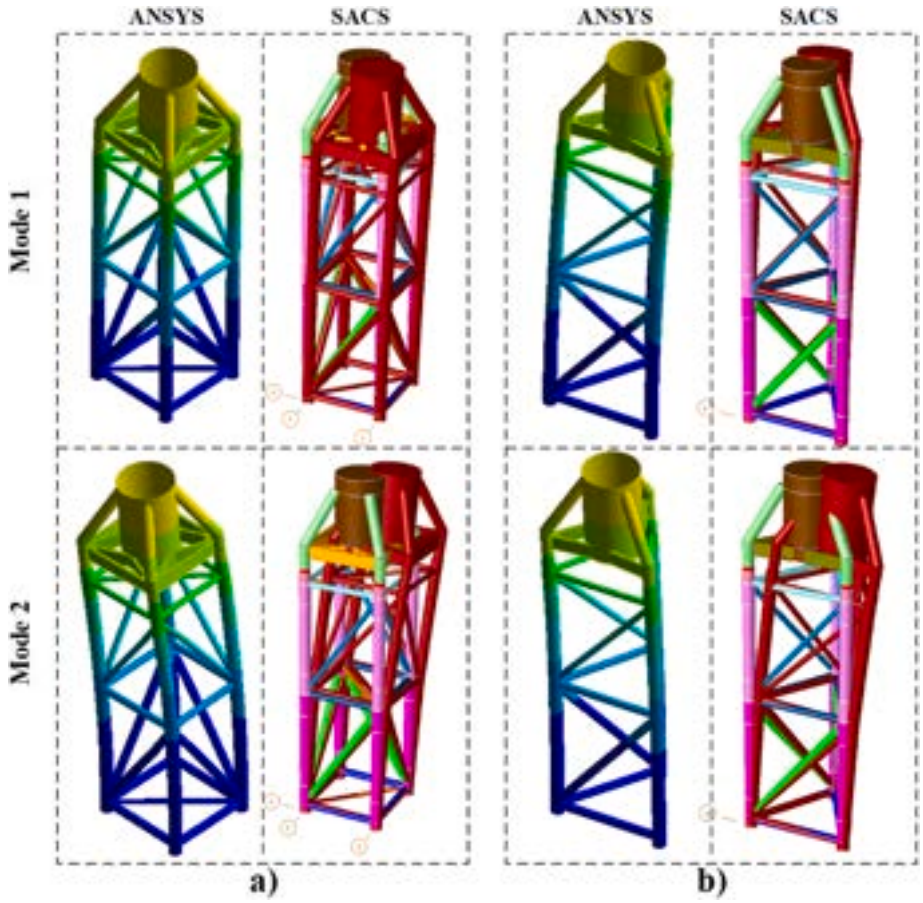

Fig. 7. Comparison of natural frequencies between ANSYS and SACS models: (a) 4LJ-P and (b) 3LJ-P.

Fig. 4c.

Using the above process, a new 3-legged jacket substructure with Pratt bracing system (3LJ-P) is developed. The properties of the designed model are tabulated in Table 4, with some modifications of the transition piece. Essentially, the 4LJ-P is an existing model obtained from the Southwest Sea Offshore Wind project, and more details can be found in the POSCO report (POSCO, 2017).

For a better comparison, the total height of the transition piece (TP) and the jacket system of the developed model is the same as the existing model, approximately 32.5m above the seabed. The material for the support structure is EN S355 steel with a density of 7850 $kg/\ m^3$, the yield stress of 355 MPa, an elastic modulus of 210×10^3 MPa, and Poison's ratio of 0.3.

3.2. Numerical modeling of the jacket substructures

In this study, jacket modelings are generated using both SACS (Structural Analysis Computer System) (Bentley, 2019) and Ansys (2020) softwares. Detailed descriptions of the support structures are described in the following subsections.

3.2.1. Structural modeling by SACS

The support structure includes tower, transition piece, and jacket substructure, as shown in Fig. 5a. The wind tower is modeled using the Euler-Bernoulli beam element, and it is subdivided into 22 elements. To accurately describe the dynamic behavior of OWT, the effects of RNA and flanges are also considered. The RNA mass is assigned at the tower top, and the flange masses are incorporated into the numerical model by lumping them along the tower (Fig. 5b).

Beam elements are also utilized for the transition piece modeling. The TP is assembled using the hollow circle tube and the "H" shape sections. For the simplicity, however, the door on the cylinder is neglected in the modeling.

Like the tower modeling, use of beam elements is also applied for the modeling of the jacket substructures. Hollow circular sections are used for the main jacket members. These sections are classified based on their diameters and thicknesses listed in Table 4. Effects of the joint-can and overlap are also considered. The former is modeled by increasing the diameter and thickness of the leg member at its connections; thus, the leg member is divided into three segments, as shown in Fig. 5c. The latter is the connection between the jacket and brace members. Without considering this aspect, the duplication of the brace members may distort the overall structural response (Fig. 5c) (Shi et al., 2013b). Moreover, in order to connect the jacket pile and jacket leg together, the wishbone (WB) element is adopted. The WB is a dummy element, and its density is given as zero. More detailed information of the WB element can be found in the SACS manual (Bentley, 2019). The WB element allows the jacket pile and jacket leg to slide past one another, thus the pile can fall freely along its vertical axis. In this study, the soil-pile interaction is ignored; thus, the numerical models are assumed to be fixed at the bottom of the jacket substructure.

Table 5
Comparison of natural frequencies between ANSYS and SACS [Hz].

	4LJ-P			3LJ-P		
Mode	ANSYS	SACS	Diff. (%)	ANSYS	SACS	Diff. (%)
1	2.32	2.43	4.50	2.49	2.60	4.35
2	3.04	3.07	0.89	2.49	2.60	4.35

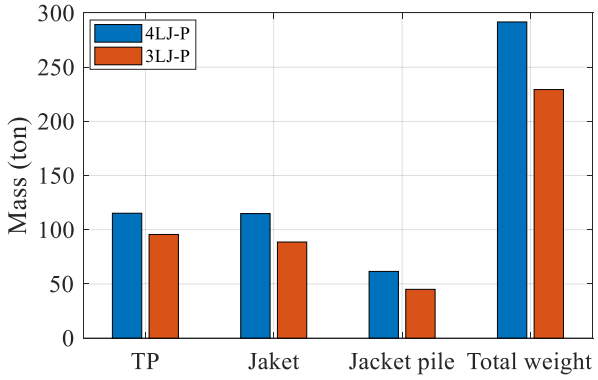

Fig. 8. Comparison of the mass.

3.2.2. Structural modeling by ANSYS

In this study, the jacket substructures are developed with some modifications of the transition piece. Therefore, a large stress distribution may occur at this component due to the transferring of loads from the tower to the jacket substructure. In order to capture local stress concentration (LSC) accurately, the ANSYS software package is introduced for jacket modeling.

The structural modeling consists of a jacket structure and transition piece, as shown in Fig. 6. The jacket substructure is modeled by the shell element (SHELL181), which is suitable for checking the LSC locations. The structural properties are taken from Table 4. The additional 10 m of the tubular tower has been included to simulate the transferring of design loads from the wind tower to the jacket substructure. The quadrilateral method is applied for the meshing of structural members and the rigid Multi-Point Constraint (MPC) method is applied at the IP. The purpose of the MPC is to get the coupling between the transition piece and the tower.

3.2.3. Comparison of SACS and ANSYS models

Modal analyses are performed for jacket structures to identify the differences between SACS and ANSYS models. The mode shapes are compared in Fig. 7. In general, the outcomes obtained from these calculations are identical. The corresponding natural frequencies are tabulated in Table 5. As seen, the ANSYS modeling has relatively well agreements with SACS modeling. In the case of 4LJ-P, the differences between SACS and ANSYS modeling are 4.5% and 0.89% for mode 1 and mode 2, respectively; whereas, a value of 4.35% is found for 3LJ-P.

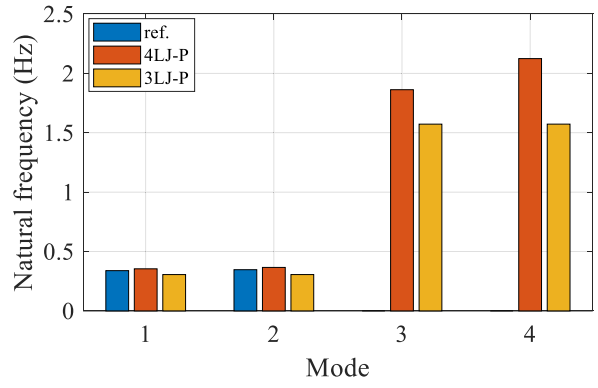

Fig. 9. Comparison of the natural frequencies.

4. Feasibility analysis

Feasibility analysis is studied for various topologies of jacket substructures (i.e., 4LJ-P and 3LJ-P), aiming to select a more efficient jacket substructure for the existing offshore wind turbine. In which, the existing 4LJ-P is a 2-layer structure that has a spacing of 11.5m at the bottom layer and 10.68m at the top layer. The layer spacing of 3LJ-P is the same as 4LJ-P. All other parameters (i.e., material properties, cross-sections of leg/brace members) are also the same. The design process will cover the main requirements in terms of the target frequency and ultimate limit state. Furthermore, the mass comparison and dynamic response of jackets under extreme environmental loads are also reported.

4.1. Mass of jacket substructures

A mass comparison is performed for all jacket substructures, as plotted in Fig. 8. It is observed that the total weight of 3LJ-P is about 21% smaller than that of the 4LJ-P. In particular, masses of the transition pieces are 115.2 ton and 95.6 ton for 4LJ-P and 3LJ-P, respectively, showing a difference of 17%. This trend is also the same for the jacket structure and jacket pile, with 23% and 27% differences, respectively.

In addition, the number of welded joints that affect the manufacturing and fabrication costs are also compared. In the case of 4LJ-P, there is a total of 24 joints including 16 K-joints and 8 Y/T-joints. On the other hand, a 25% reduction in the number of welded joints is found for 3LJ-P (12 K-joints and 6 Y/T-joints).

4.2. Dynamic characteristics

Modal analysis is the first step in designing an offshore wind turbine system, aiming to find the target frequencies of the whole system. As stated by Muskulus and Schafhirt (2014), the developed support structures should be far from the rotor rotational frequency (1P) and blade passing frequency (3P) ranges. This is necessary to avoid the resonance during the operation condition of the OWT.

To evaluate influences of the jacket configuration on the dynamic characteristics of OWTs, comparative modal analysis is performed. Fig. 9 and Fig. 11 show the natural frequencies and their associated mode shapes for the first four modes of the support structures. The results in Fig. 9 reveal that there is minor variation between the developed 4LJ-P and the reference solution, with a maximum difference of 5.5% in the two horizontal directions, hence, verifying the numerical modeling. A comparison of structural frequencies with typical external force spectra is given in Fig. 10. The spectra are characterized by the site data given in Table 2. The Kaimal and JONSWAP spectra are used for the

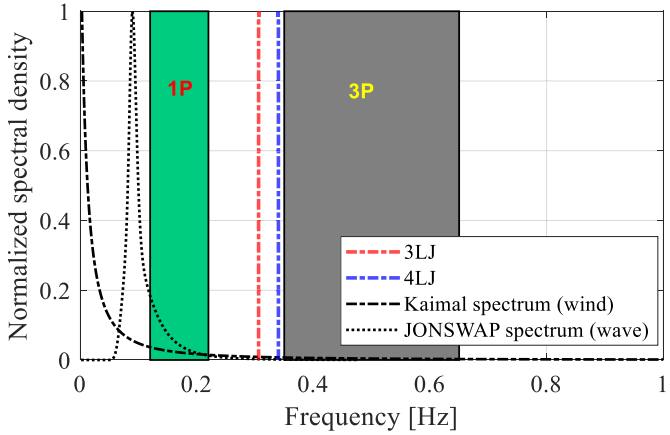

Fig. 10. Frequency diagram of jacket substructures and external forces.

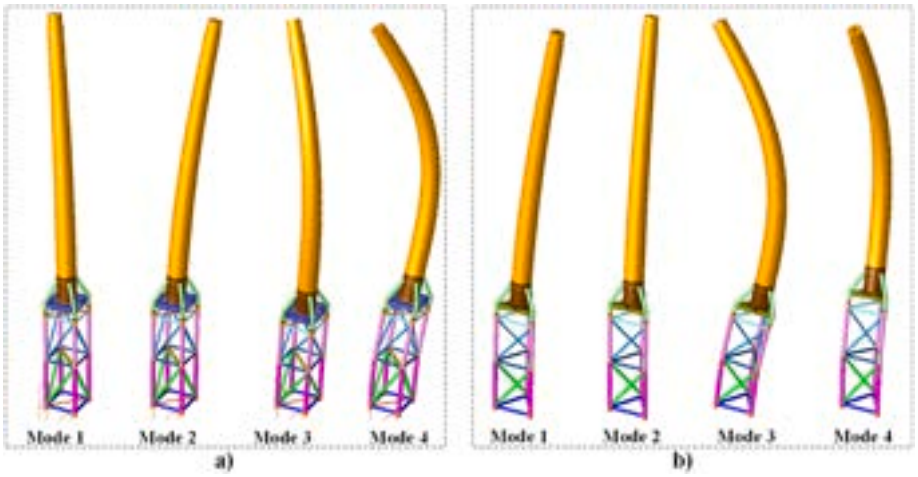

Fig. 11. First four vibration mode shapes of the support structures: (a) 4LJ-P and (b) 3LJ-P.

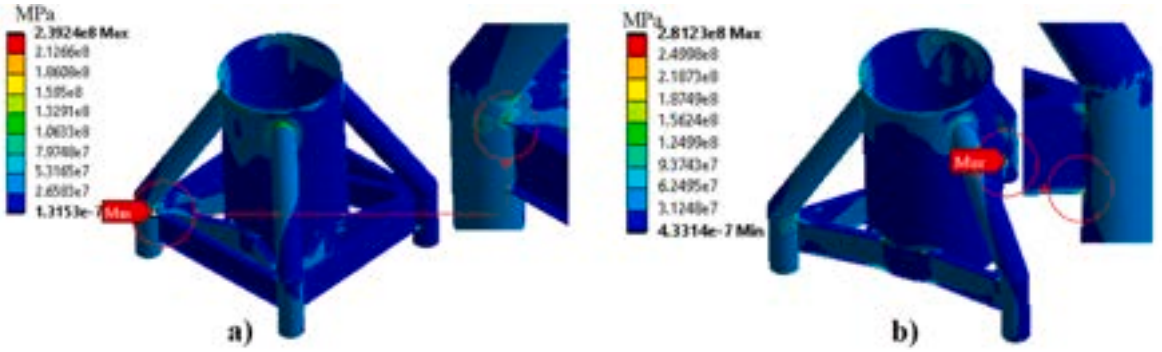

Fig. 12. Von Mises stress distribution in the transition piece under DLC1: (a) 4LJ-P and (b) 3LJ-P.

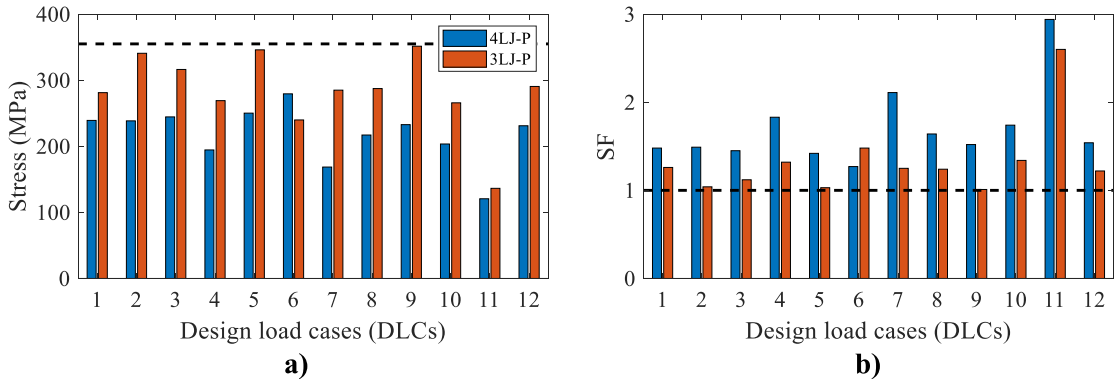

Fig. 13. Histograms of (a) maximum stress and (b) *SF* of the transiton piece under DLCs.

wind and wave, respectively. Details of the calculation can be found in Refs. (Amin et al., 2021b, 2021a; DNVGL, 2014).

Comparing to the 4-legged system, the natural frequencies of the 3-legged system are decreased due to the stiffness decrement, as expected. The first and second frequencies shift leftward, with decrements of 13.7% and 16.4%, respectively. It is known that 3LJ-P is the designing soft-stiff system, which can avoid the resonance effect. Furthermore, the eigenvalues of higher modes are in the stiff-stiff range, with the same value of 1.58Hz for the third and fourth modes. This observation indicates that the newly developed 3-legged system is acceptable for the structural analysis in the following studies.

The difference in natural frequencies of the support structures is because of variations in their mass and stiffness properties. As pointed out by Jalbi and Bhattacharya (2018), the support structure can be assumed as an equivalent Single Degree of Freedom (SDOF) system. As a result, the first natural frequency can be defined as a function of the equivalent stiffness (K_{eq}) and equivalent lumped mass (M_{eq}). Using this relation, the equivalent stiffnesses of 4LJ-P and 3LJ-P are achieved with the corresponding values of 2.92×10^4 kN/m and 1.97×10^4 kN/m. As expected, 3LJ-P is more flexible with a decrement of 33% in structural stiffness.

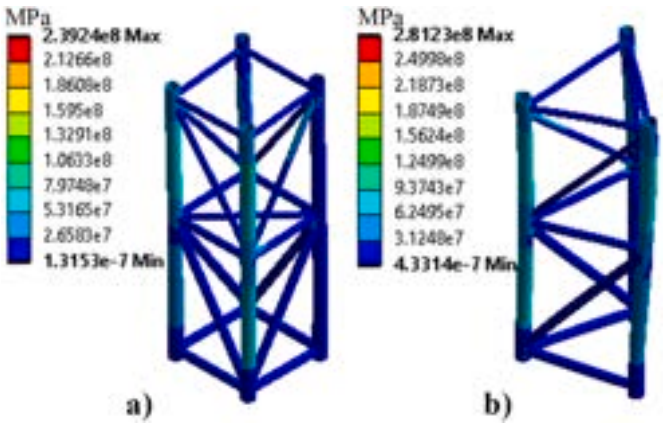

Fig. 14. Von Mises stress distribution of jacket structure under DLC1: (a) 4LJ-P and (b) 3LJ-P.

4.3. Structural performances under design load cases (DLCs)

The jacket substructures are analyzed with all DLCs given in Section 2.3. This aims to ensure the maximum stress of the selected jacket member is within a sufficient capacity. Fig. 12 shows an example of von Mises stress distribution of 4LJ-P and 3LJ-P under DLC1. The results indicate that von Mises stress of the 3-legged system is larger than the 4-legged system, with a difference of 17.6%. Locations of the stress concentrations are found at the connection between transition piece and leg members. The von Mises stress distributions at the TPs under twelve DLCs are graphically displayed in Appendix (Fig. 27).

A full comparison of the maximum stress is summarized in Fig. 13a. The outcomes obtained from 3LJ-P are higher than those from 4LJ-P, with an average difference of 31%. These results are compared with the yield strength of EN S355 steel, which is represented by the horizontal dashed line. It indicates that the stresses of the developed jacket substructures are below the material yield strength limit, satisfying the ultimate design criteria.

For a better comparison, the safety factor of the transition piece is recommended and this is calculated as follows (IEC 61400-1, 2005):

$$SF = \frac{\sigma_y}{\sigma_m} \tag{5}$$

in which, σ_y is the yield stress of the material; σ_m is the maximum stress from the analysis, which is obtained from the von Mises stress distribution. Fig. 13b displays the *SF* achieved from both jacket substructures. As seen in the figure, the obtained safety factors are larger than one, implying the design satisfaction of the selected members.

With regards to the jacket structures, a comparison of von Mises stresses is shown in Fig. 14. As seen in the figure, these structures satisfy the ULS requirements. Due to reduction of jacket leg numbers, higher stress values are found in the case of 3LJ-P, as shown in Fig. 15.

4.4. Structural performances under environmental loads (Env)

Displacements at the interface point (IP) of both 4LJ-P and 3LJ-P under various environmental loading directionality are shown in

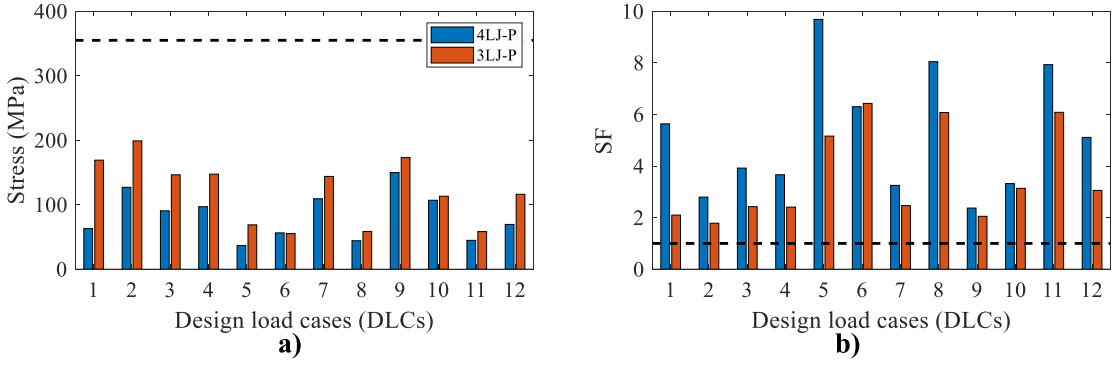

Fig. 15. Histograms of (a) maximum stress and (b) *SF* of the jacket structure under DLCs.

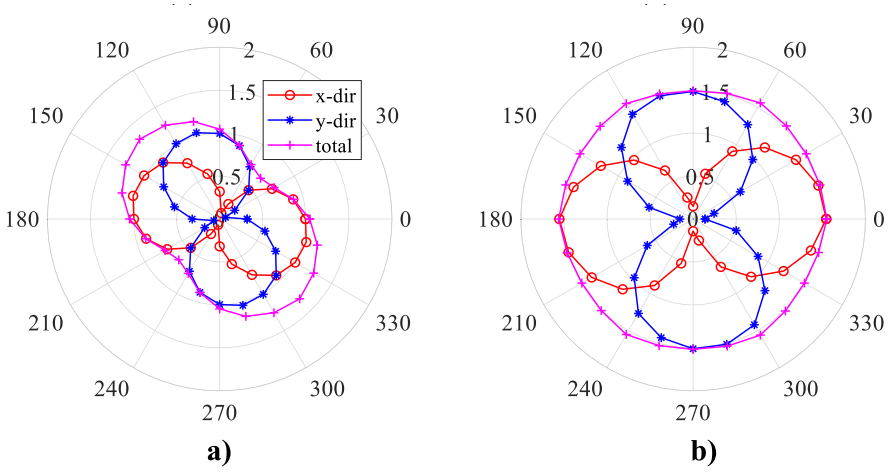

Fig. 16. Polar diagrams of the lateral displacements for the jacket substructures: (a) 4LJ-P and (b) 3LJ-P [cm].

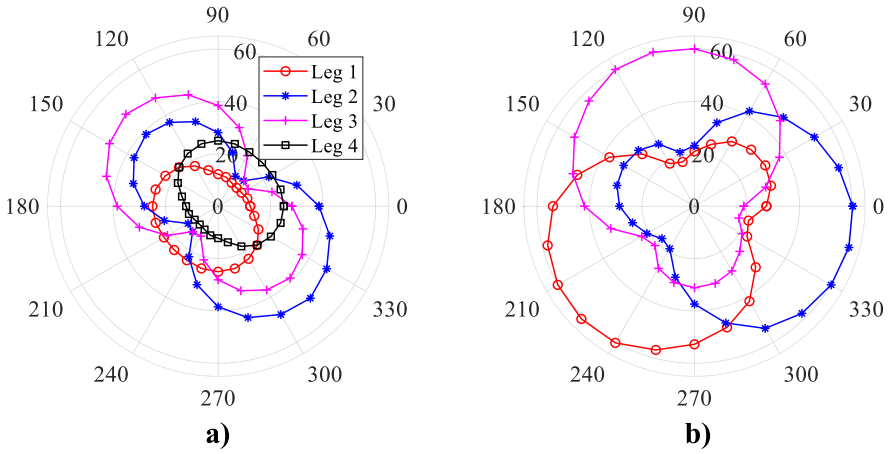

Fig. 17. Polar diagrams of the stresses for the jacket substructures: (a) 4LJ-P and (b) 3LJ-P [MPa].

Fig. 16. These polar diagrams describe very significant findings. As seen, the maximum displacements of 4LJ-P are dependent on the input loading directions (Fig. 16a). The critical response is found at the loading directionality of 135 ° and 315 ° with a maximum displacement of 1.31 cm. On the contrary, the responses of 3LJ-P are almost independent of the environmental loading directionality (Fig. 16b); thus, the total response is a circle in the polar diagram. These outcomes demonstrate that considering the influence of loading directionality is not necessary in the case of 3LJ-P.

Similar observations are made for the stresses at the lower jacket legs, as shown in Fig. 17. In the case of 3LJ-P, stress distribution of each jacket leg produces very similar trends, with a maximum value of about 60 MPa. In contrast, stresses of the 4LJ-P modeling are separated into two groups having the same trend (i.e. group 1 for leg 1 - leg 4, and group 2 for leg 2 - leg 3). The maximum stress of group 1 is about 50 MPa. While in the case of group 2, the maximum responses decrease by about 50%. Similar to the displacement results, the peaks in the polar diagram occur at the loading orientation of 135 ° and 315 ° for the 4LJ-P.

5. Sensitivity analysis of the 3-legged jacket substructure

Efficiency of the 3LJ substructure is substantiated in Section 4. In this section, parametric studies are carried out to investigate effects of the bracing systems on the dynamic performance of the 3LJ substructure. Various traditional jacket substructures, including 3LJ-P (Pratt), 3LJ-W (Warren), and 3LJ-X (X-brace), are established as shown in Fig. 18. Notably, the structural parameters (i.e., material properties, sections of leg and brace members, and height of each layer) are the same, except the bracing layout.

5.1. *Influence of bracing layouts to the masses of jacket substructures*

Mass of three jacket substructures are compared in Fig. 19. It is worth mentioning that the total weights obtained from 3LJ-P and 3LJ-W are the same, with a value of 229 ton. They are also the same for the individual components (i.e., TP, jacket structure, and jacket pile). In case of the X-type topological substructure, however, the structural mass is slightly larger (around 4.8%) comparing to the other layouts.

The same finding is found for the number of welded joints. In the case of 3LJ-X, there is a total of 24 joints including 12 K-joints, 6 Y/T-joints,

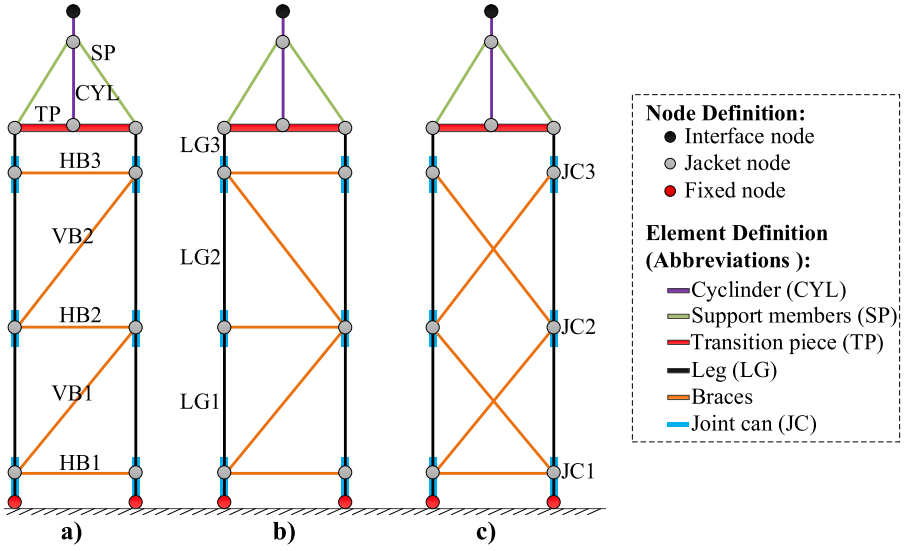

Fig. 18. Various bracing layouts of 3LJ substructure: (a) 3LJ-P, (b) 3LJ-W, and (c) 3LJ-X.

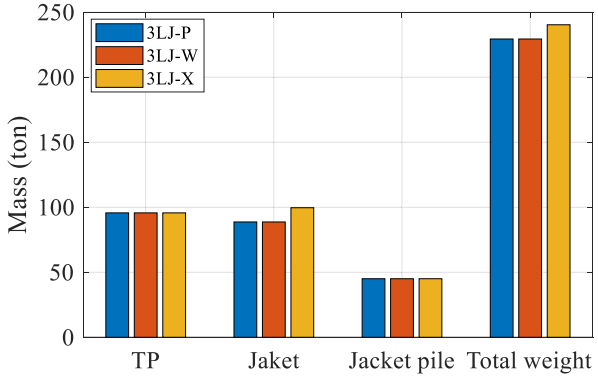

Fig. 19. Masses of three jacket substructures.

and 6 X-joints. In contrast, a 25% reduction in the number of welded joints is found for 3LJ-P (12 K-joints and 6 Y/T-joints), as well as 3LJ-W (9 K-joints and 9 Y/T-joints).

5.2. Influence of bracing layouts to the natural frequencies

Table 6 lists natural frequencies of the first six modes of the support structures. Compared to the 3LJ-P, eigenvalues of the first and second modes obtained from 3LJ-W are almost the same, and the changes are miniscule for higher modes with an average difference of less than 1%. In contrast, natural frequencies of the X-bracing form have slight increases, especially for the higher modes with values of up to 7% due to increase of the structural properties (i.e., equivalent stiffness and mass properties).

Using formulas obtained from Jalbi and Bhattacharya (2018), structural properties of the three support structures are calculated, as given in Fig. 20. As seen, these parameters are the same for Pratt and Warren bracing forms, and the computed values of effective stiffness and mass are 1.97×10^4 kN/m and 542.0 ton, respectively. In addition, the X-bracing system provides higher properties comparing to the others, with increases of 3.2% and 4.8% for the equivalent stiffness and mass, respectively.

5.3. Performances of three jacket bracing configurations under DLCs

The maximum stresses at the TP are obtained and compared to each other in order to evaluate the load-carrying capacity of the three jacket models. It is noted that the geometric parameters of these models are the same. Graphical examples of the stress distribution and their corresponding locations occurring on the TP are shown in Fig. 21. Comparisons of the maximum stresses of TP and their corresponding *SFs* under all DLCs are summarized in Fig. 22. As seen, the maximum von Mises stresses of 3LJ-W and 3LJ-X are close to those of the 3LJ-P, with average differences of 8.2% and 7.7%, respectively. However, under force in Y-direction (DLC9), the W-type has the lowest flexural capacity (Fig. 21b). The maximum stress of 3LJ-W can be decreased by (1) increasing its thickness, or (2) adding the stiffness members.

Table 6
Natural frequencies of three support structures [Hz].

Mode	3LJ-P	3LJ-W	3LJ-X
1	0.306	0.306	0.308
2	0.306	0.306	0.308
3	1.572	1.585	1.695
4	1.572	1.585	1.695
5	3.339	3.366	3.688
6	3.339	3.366	3.690

Similar to the transition piece, von Mises stress distributions of the three jacket structures are also evaluated. The comparison is given in Fig. 23. In general, the stress distributions at the leg members are higher than those of bracing members. This is since jacket members are tension-compression systems, aiming to transfer loads from the TP to the pile foundation; while the key function of the bracing systems is to resist the deformation of the whole jacket systems. More detailed stress distributions of the jacket structures under DLCs are shown in Appendix (Fig. 28) and the maximum stresses are summarized in Fig. 24. The analysis results show that all jacket members satisfy the ULS requirements.

5.4. Performances of three jacket bracing configurations under Env

A comparison of total displacements (defined in Eq. (1)) of the three bracing topological forms under Env is given in Fig. 25. As seen in the figure, the displacements are almost independent to the loading directionality, and the minimum response belongs to X-brace. Thus, responses of the three jacket structures are circles in the polar diagram. The average displacements are 1.52 cm, 1.46 cm, and 1.01 cm for Pratt, Warren, and X-bracing topological forms, respectively. The discrepancy is primarily due to the structural configuration, leading to a variation in the global stiffness of the jacket substructures, which is already explained in section 5.2.

A detailed comparison of stresses for each leg member is illustrated in Fig. 26. The results indicate that there is no difference in the maximum stresses between Pratt and Warren systems. The maximum response is about 61 MPa for all leg members. On the contrary, due to its higher stiffness, a smaller response is found in the X-bracing system, with a decrement of up to 23%.

6. Major observations and limitations

6.1. Observations

The major results obtained from the feasibility analysis are summarized as follows:

- In comparison with the existing 4LJ-P substructure, 3LJ-P is more effective with a reduction of up to 16.4% on natural frequencies. Dominant frequencies of 3LJ-P fall within the soft-stiff design, which can avoid the structural resonance.
- The developed 3LJ substructure shows large differences in structural properties (i.e., stiffness and mass) comparing to 4LJ-P, which have significant impacts on their dynamic characteristics. Reductions of up to 33% and 21% for the stiffness and mass are found in the case of 3LJ-P.

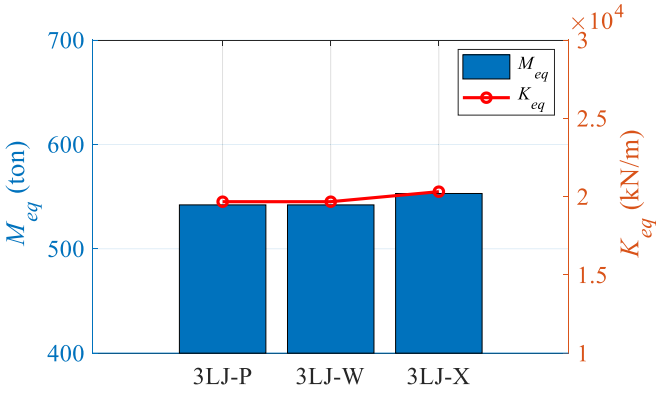

Fig. 20. Structural properties of three support structures.

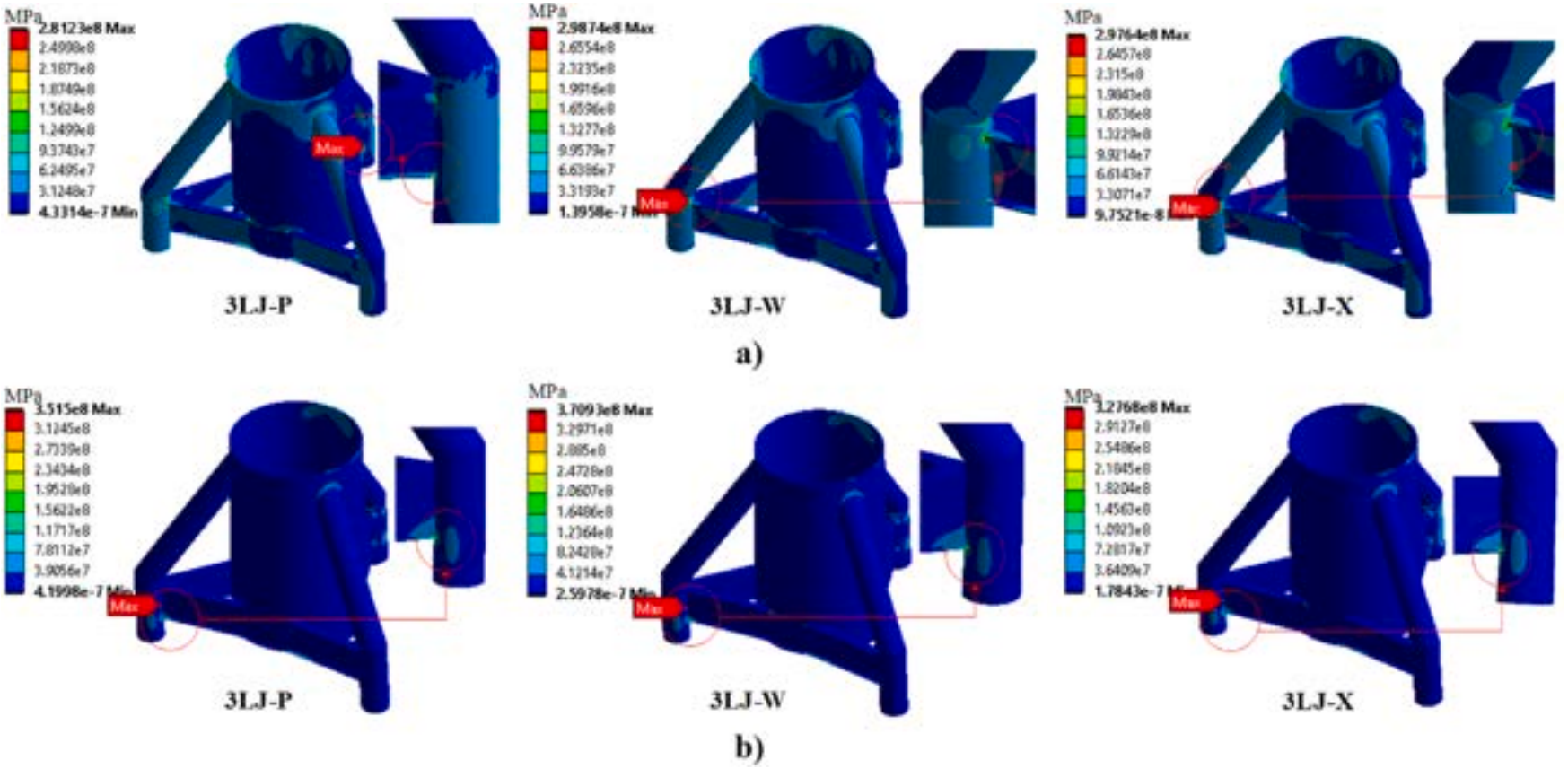

Fig. 21. Von Mises stress distribution of transition piece under (a) DLC1 and (b) DLC9.

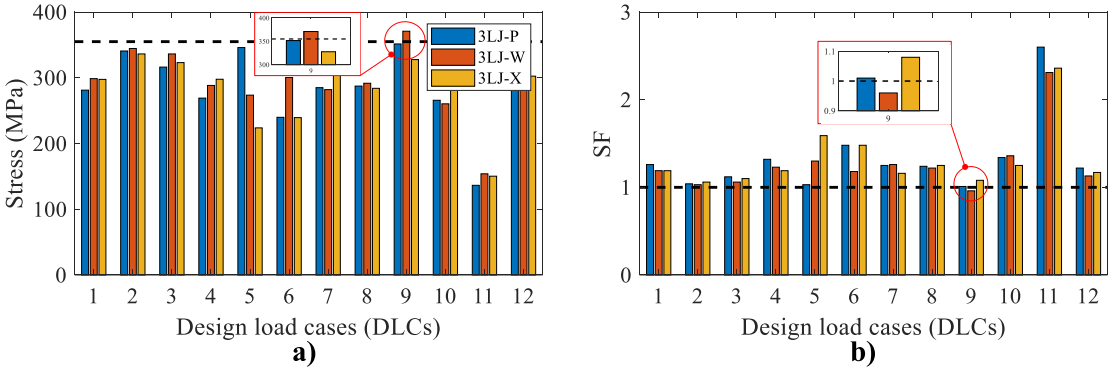

Fig. 22. Histograms of (a) stress and (b) *SF* of transiton piece under DLCs.

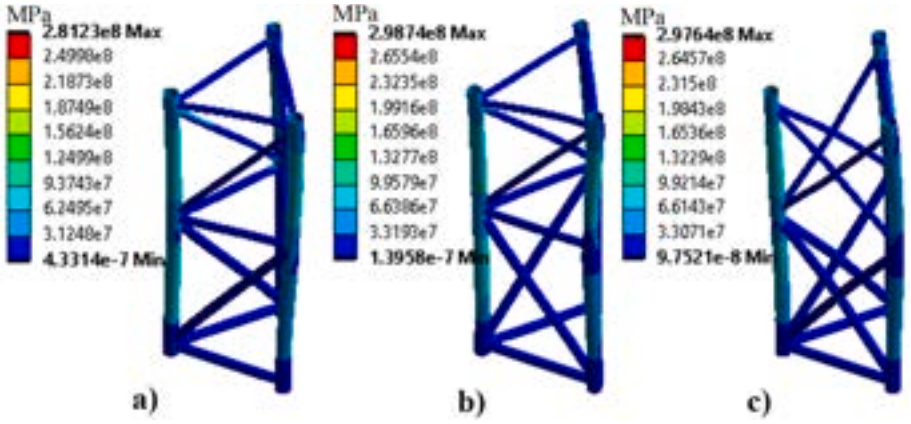

Fig. 23. Stress distribution of jacket substructures under DLC1: (a) 3LJ-P, (b) 3LJ-W, and (c) 3LJ-X.

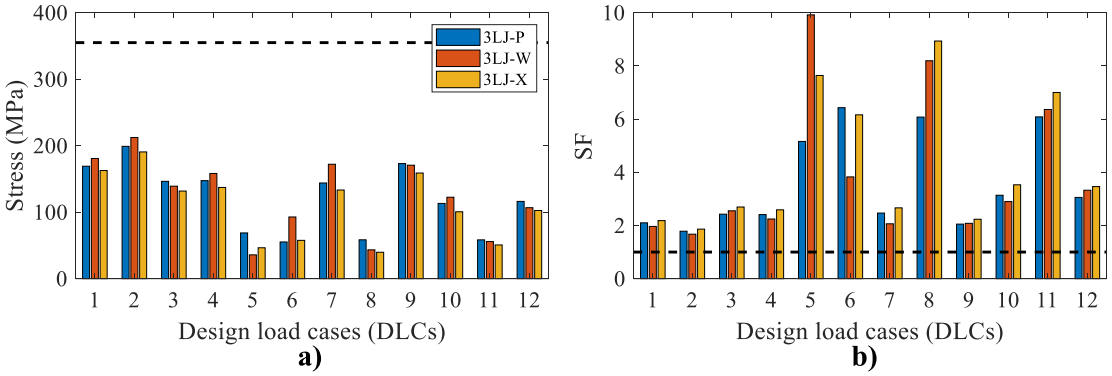

Fig. 24. Histograms of (a) stress and (b) *SF* of jacket structure under DLCs.

- The polar diagrams show that 4LJ-P has a strong polarization with the environmental loading directionality, while they are almost independent in the case of 3LJs.

The outcomes from the sensitivity analysis highlight the following findings:

- Among the three 3LJ substructures, the X-bracing layout shows an increase in stiffness (3.2%), together with increases in material consumption (4.8%) and number of welded joints (25%).
- Dynamic characteristics of the three 3LJs show slight differences each other. In comparison to the 3LJ-P, the differences in natural frequencies of 3LJ-W and 3LJ-X are less than 1% for first two modes and 7% for the third and fourth modes.
- Under DLCs, the maximum von Mises stress of 3LJ-W caused by local stress concentration at TP is slightly larger (5.5%) than the material yield capacity, while the other layouts (3LJ-P and 3LJ-X) satisfy all the ULS requirements.

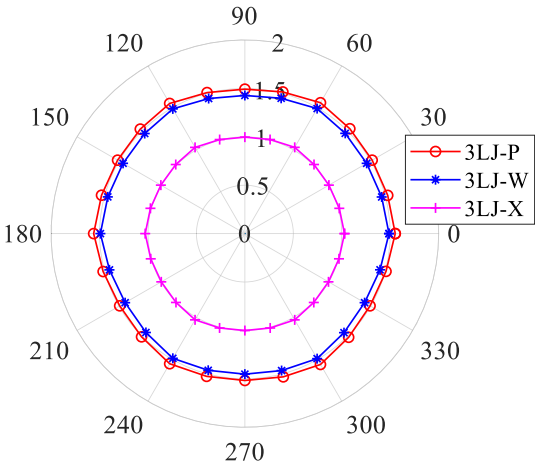

Fig. 25. Polar diagram of total displacements for 3LJs [cm].

- The 3-legged jacket substructure is more effective in comparison with the existing 4LJ-P substructure. The 3LJ reduces efficiently the manufacturing and fabrication costs in comparison with the existing 4-legged jacket substructure, material cost and number of welded joints can be saved up to 21% and 25%, respectively. Moreover, the polar diagrams show that 3LJ is almost independent with the environmental loading directions, while there is a strong polarization in the case of 4LJ-P.
- The dynamic performances of the jacket substructures are significant affected by the bracing topological forms. In three bracing types of 3LJs, the X-type has the highest flexural stiffness, as well as a 25% increment of welded joints compared to other bracing types. In contrast, P- and W-bracing types have lower flexural capacity. Among these, W-type reaches its ultimate strength earlier than P-type although the other conditions (i.e., natural frequencies, responses against Env, and material consumptions) are basically the same. Therefore, if 3LJ is selected, it is recommended to use the Pratt bracing system, which has the best performance under the considered loading conditions.

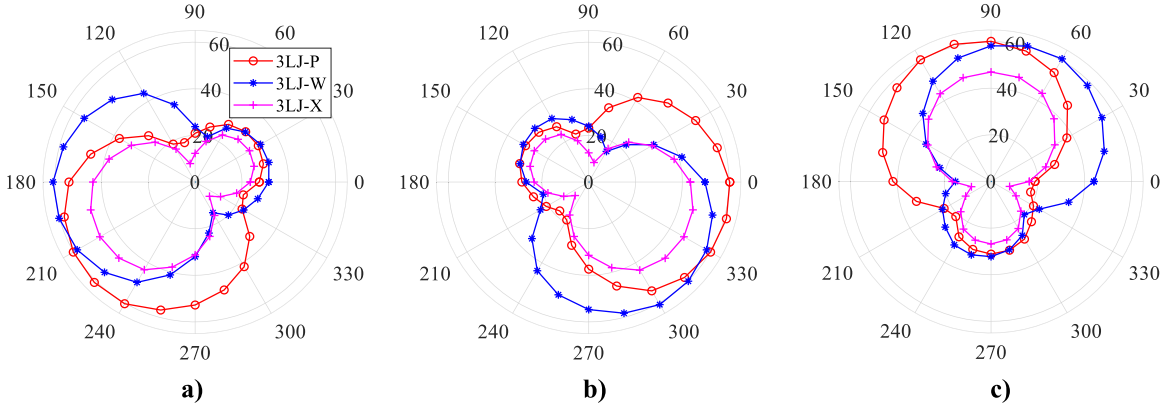

Fig. 26. Polar diagram of stresses for the jacket legs: (a) leg 1, (b) leg 2, and (c) leg 3 [MPa].

6.2. Limitations

In this study, the developed jacket substructures are examined with several main design requirements (i.e., target frequency, material cost, and dynamic characteristics under Env and DLCs) and it can be used as the preliminary design. For the final stage of design process, further studies such as design of jacket joints (joint can), global buckling check, fatigue design, serviceability limit check, and check of accident limit such as boat impact, etc. are required. Additionally, the angles between leg and brace members of 3LJ-P are smaller than those of 4LJ-P; thus, more attention is required for joint detailing. The findings in this study might be useful to the engineers who are working on the development of large-scaled OWTs for the upcoming offshore wind farms in Korea.

7. Conclusions

The main objective of this study is to develop a more cost-effective jacket substructure for offshore wind. To meet this objective, three 3-legged jacket substructures with various topological bracing forms (i.e., Pratt, Warren, and X-bracing) are developed based on reference 4-legged jacket substructure. Feasibility and Sensitivity Analyses (FSA) are also carried out to explore the reasonable jacket topological substructure. The general conclusions can be drawn as follows:

CRediT authorship contribution statement

Thanh-Tuan Tran: Writing – original draft, Conceptualization, Methodology, Visualization, Validation. **Eungsoo Kim:** Data curation. **Daeyong Lee:** Software, Methodology, Writing – review & editing, Supervision.

Declaration of competing interest

The authors declare that they have no known competing financial interests or personal relationships that could have appeared to influence the work reported in this paper.

Acknowledgment

This work was supported by the National Research Foundation of Korea (NRF) grant funded by the Korean government (Ministry of Science and ICT) (No. 2021 R1F1A1046912) and by Basic Science Research Program through the National Research Foundation of Korea (NRF) funded by the Ministry of Education (NRF 2021R1A6A1A0304518511).

Appendix

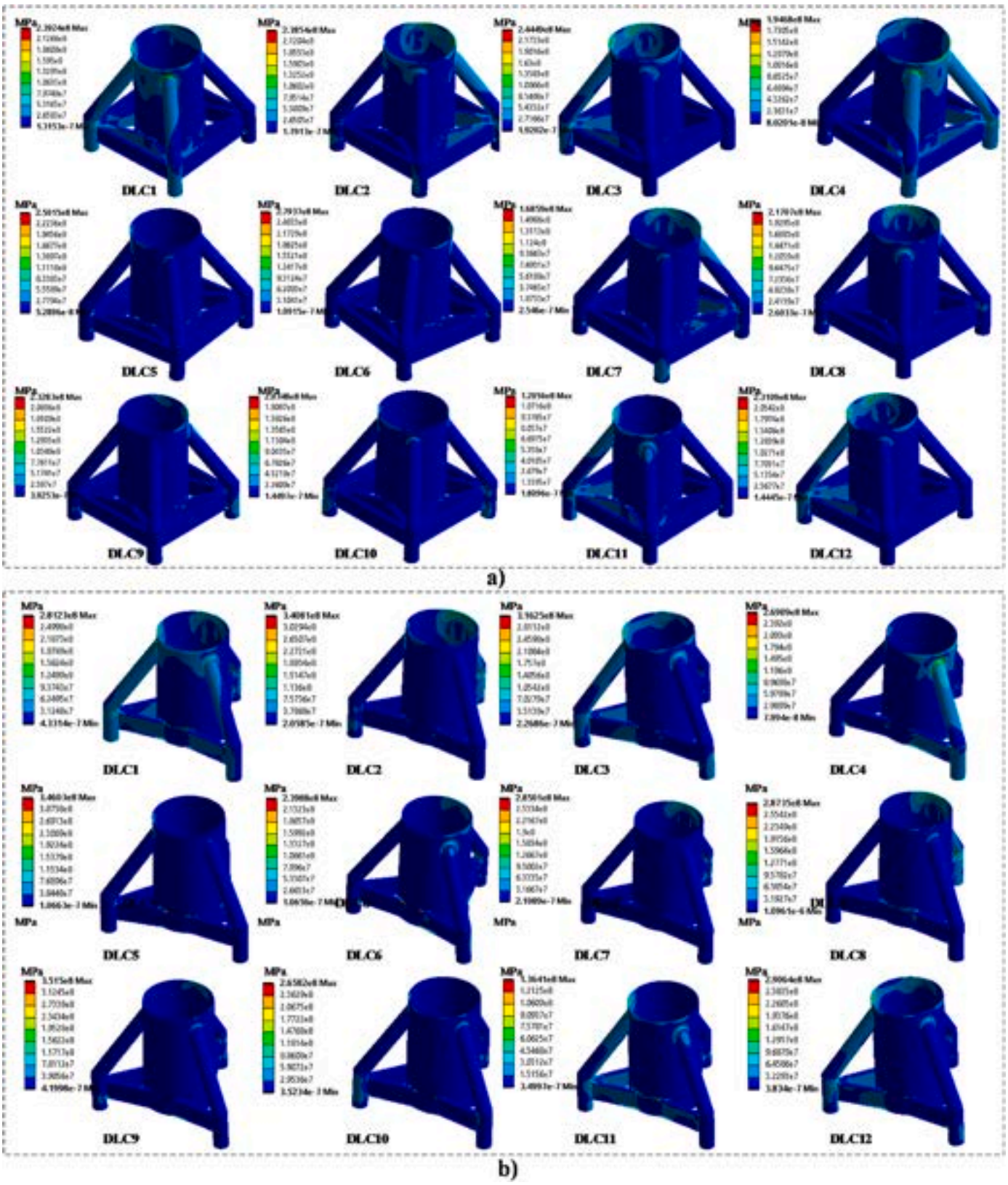

Fig. 27. Stress distribution of the transition pieces under DLCs: (a) 4LJ-P and (b) 3LJ-P [MPa].

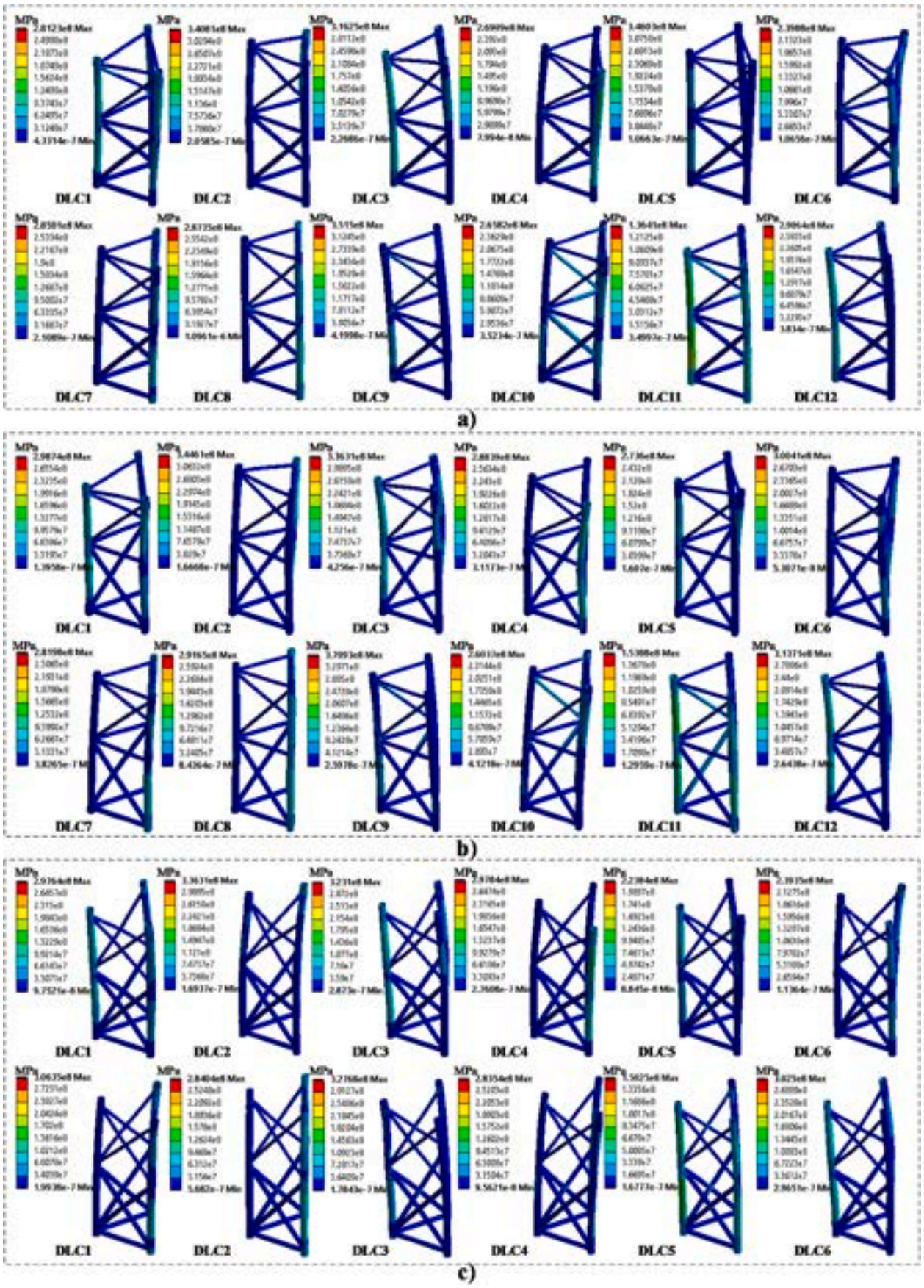

Fig. 28. Stress distribution of the jacket substructures under DLCs: (a) 3LJ-P, (b) 3LJ-W, and (c) 3LJ-X [MPa].

References

Álamo, G.M., Aznárez, J.J., Padrón, L.A., Martínez-Castro, A.E., Gallego, R., Maeso, O., 2018. Dynamic soil-structure interaction in offshore wind turbines on monopiles in layered seabed based on real data. Ocean Eng. 156, 14–24. https://doi.org/10.1016/J.OCEANENG.2018.02.059.

Amin, I., Ali, M.E.A., Bayoumi, S., Balah, A., Oterkus, S., Shawky, H., Oterkus, E., 2021a. Numerical hydrodynamics-based design of an offshore platform to support a desalination plant and a wind turbine in Egypt. Ocean Eng. 229, 108598 https://doi.org/10.1016/J.OCEANENG.2021.108598.

Amin, I., Dai, S., Day, S., Ali, M.E.A., Balah, A., Shawky, H., Oterkus, S., Oterkus, E., 2021b. Experimental study on the motion response of an integrated floating desalination plant and offshore wind turbine on a non-ship platform. Ocean Eng. 234, 109275 https://doi.org/10.1016/J.OCEANENG.2021.109275.

Ansys, 2020. Academic Research Mechanical, Release 2020R1, Help System, Coupled Field Analysis Guide. ANSYS, Inc.

Bentley, 2019. Structural Analysis Computer System (SACS), vol. 14. User's Manual, Release, Engineering Dynamics version 0.

Bhattacharya, S., 2019. Design of Foundations for Offshore Wind Turbines. Wiley, PO19 8SQ, UK.

Bossanyi, E., 2010. GH-bladed Version 4.0 User Manual.

Chew, K.-H., Eddie, Y.N., Tai, K., 2014. Offshore Wind Turbine jacket substructure: a comparison study between four-legged and three-legged designs. J. Ocean Wind Energy 1, 74–81.

DNVGL, 2014. DNVGL-DNV-OS-J101 - Design of Offshore Wind Turbine Structures.

Häfele, J., Damiani, R.R., King, R.N., Gebhardt, C.G., Rolfes, R., 2018. A systematic approach to offshore wind turbine jacket predesign and optimization: geometry, cost, and surrogate structural code check models. Wind Energy Sci 3, 553–572. https://doi.org/10.5194/wes-3-553-2018.

Häfele, J., Gebhardt, C.G., Rolfes, R., 2019. A comparison study on jacket substructures for offshore wind turbines based on optimization. Wind Energy Sci 4, 23–40. https://doi.org/10.5194/wes-4-23-2019.

IEC 61400-1, 2005. Wind Turbines-Part 1: Design Requirements.

Jalbi, S., Bhattacharya, S., 2020. Concept design of jacket foundations for offshore wind turbines in 10 steps. Soil Dynam. Earthq. Eng. 139, 106357 https://doi.org/10.1016/j.soildyn.2020.106357.

Jalbi, S., Bhattacharya, S., 2018. Closed form solution for the first natural frequency of offshore wind turbine jackets supported on multiple foundations incorporating soil-structure interaction. Soil Dynam. Earthq. Eng. 113, 593–613. https://doi.org/10.1016/j.soildyn.2018.06.011.

Ju, S.H., Huang, Y.C., 2019. Analyses of offshore wind turbine structures with soil-structure interaction under earthquakes. Ocean Eng. 187, 106190 https://doi.org/10.1016/J.OCEANENG.2019.106190.

Muskulus, M., Schafhirt, S., 2014. Design optimization of wind turbine support structures — a review. J. Ocean Wind Energy 1, 12–22.

Norsok, 2004. Standard Design of Steel Structure. DNV.

Plodpradit, P., Dinh, V.N., Kim, K.-D., 2019. Coupled analysis of offshore wind turbine jacket structures with pile-soil-structure interaction using FAST v8 and X-SEA. Appl. Sci.Jeollabuk-do 9 (1633 9), 1633. https://doi.org/10.3390/APP9081633.

POSCO, 2017. 4-Leg Jacket Substructure for 3MW Offshore Wind Turbine, Structural Design Report.

Shi, W., Han, J., Kim, C., Lee, D., Shin, H., Park, H., 2015. Feasibility study of offshore wind turbine substructures for southwest offshore wind farm project in Korea. Renew. Energy 74, 406–413. https://doi.org/10.1016/j.renene.2014.08.039.

Shi, W., Park, H., Chung, C., Baek, J., Kim, Y., Kim, C., 2013a. Load analysis and comparison of different jacket foundations. Renew. Energy 54, 201–210. https://doi.org/10.1016/j.renene.2012.08.008.

Shi, W., Park, H., Han, J., Na, S., Kim, C., 2013b. A study on the effect of different modeling parameters on the dynamic response of A jacket-type offshore wind turbine in the Korean Southwest Sea. Renew. Energy 58, 50–59. https://doi.org/10.1016/j.renene.2013.03.010.

Tran, T.-T., Hussan, M., Kim, D., Nguyen, P.-C., 2020a. Distributed plasticity approach for the nonlinear structural assessment of offshore wind turbine. Int. J. Nav. Archit. Ocean Eng. 12, 743–754.

Tran, T.-T., Kang, S., Lee, J.-H., Lee, D., 2021. Directional bending performance of 4-leg jacket substructure supporting a 3MW offshore wind turbine. Energies 2021 14 (2725 14), 2725. https://doi.org/10.3390/EN14092725.

Tran, T.-T., Kim, E., Lee, J., Lee, D., 2020b. A study on dynamic response of 4-leg jacket structures under different sea water levels. In: Proceedings of the KWEA Fall Conference. Jeju.

Tran, Thanh-Tuan, Lee, J., Lee, D., 2020. Influence of wave/wind loading direction on dynamic response of 4-leg jacket substructures. In: KSCE 2020 Convention. Jeju.

Wu, X., Hu, Y., Li, Y., Yang, J., Duan, L., Wang, T., Adcock, T., Jiang, Z., Gao, Z., Lin, Z., Borthwick, A., Liao, S., 2019. Foundations of offshore wind turbines: a review. Renew. Sustain. Energy Rev. 104, 379–393.

Zhang, P., Li, J., Gan, Y., Zhang, J., Qi, X., Le, C., Ding, H., 2020. Bearing capacity and load transfer of brace topological in offshore wind turbine jacket structure. Ocean Eng. 199, 107037 https://doi.org/10.1016/j.oceaneng.2020.107037.